MINISTRY OF EDUCATION AND SCIENCE OF UKRAINE
V. N. KARAZIN KHARKIV NATIONAL UNIVERSITY

APPLIED PROBLEMS OF MICROFLUIDICS AND NANOFLUIDICS

Metodical recommendations
for practical course and individual work

Kharkiv – 2023

UDK 539.3 (075.8)
A 67

Reviewers:

Yu. V. Romashov – Dr. tech. sci., Professor of the Department «Vapour-Generator-Building» Kharkiv National Polytechnic University «Kharkiv Polytechnic Institution KPI»;
O. M. Datsok – PhD in technical sci., Docent of Kharkiv National Technical University of Radioelectronics.

Approved for publication by the decision of the Sientific and Methodical Council of V. N. Karazin Kharkiv National University (Protocol № 3 of February 27, 2023)

A 67 **Applied** problems of microfluidics and nanofluidics : methodical recommendations for practical course and individual work / compiler N. Kizilova. – Kharkiv : V. N. Karazin Kharkiv National University, 2020. – 32 p.

The basic knowledge of the micro/nanorheology and micro/nanofluidics are presented. The detailed solutions for the laminar flows of classical fluids between parallel plates and coaxial cylindrical tubes (both Poiseuille and Couette flows), laminar flow in an open inclined duct, Poiseuille flow in the channels with elliptic, circular, triangle and rectangle cross-sections and given. The corresponding solutions for the suspensions of microparticles (microfluids) and nanoparticles (nanofluids) of the Navier-Stokes equations with velocity slip boundary conditions of the first and second order, respectively, are presented for the most of the problems while the rest are proposed as individual tasks.

For students of mathematical and physical faculties who study nanosciences, nanotechnologies and are interested in practical skills in solving applied problems of micro/nanofluidics.

UDK 539.3 (075.8)

Навчальне видання

Кізілова Наталія Миколаївна

ПРИКЛАДНІ ЗАДАЧІ МІКРОФЛЮІДИКИ І НАНОФЛЮІДИКИ

Методичні рекомендації
до практичних занять та самостійної роботи

(Англ. мовою)

Коректор *А. І. Самсонова*
Комп'ютерне верстання *В. В. Савінкова*
Макет обкладинки *І. М. Дончик*

Формат 60x84/16. Ум. друк. арк. 1,65. Наклад 50 пр. Зам. № 87/20.

Видавець і виготовлювач
Харківський національний університет імені В. Н. Каразіна,
61022, м. Харків, майдан Свободи, 4.
Свідоцтво суб'єкта видавничої справи ДК № 3367 від 13.01.2009
Видавництво ХНУ імені В. Н. Каразіна

CONTENTS

INTRODUCTION

During the last decade the **microfluids** (suspensions of microparticles with diameters d = 10–100 μm) and **nanofluids** (suspensions of nanoparticles with diameters d = 10–100 νm) have become important components of numerous devices designed for mixing and purification of the microscopic volumes of technical and biological fluids, biochemical analysis and medical diagnostics in the lab-on-a-chip flow systems, efficient nanofluid-based microcoolers/ heaters for micro/nano rotors, gears/ engines, and many other miniaturized devices [1–3] (Fig. 1).

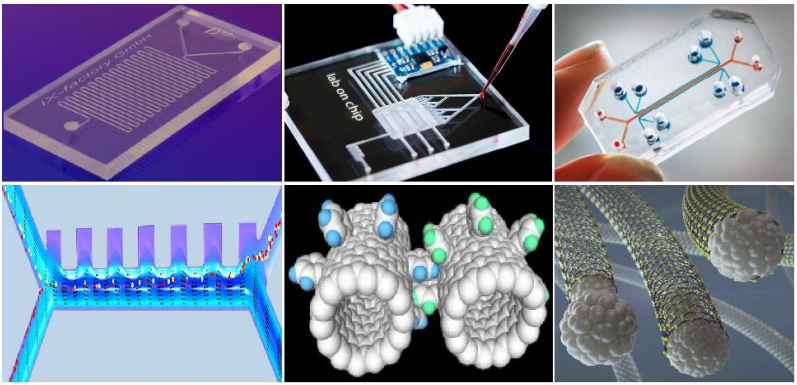

Fig. 1. Examples of micro/nanodevices

Micro and nanoscale objects are abounding in nature and technique. Typical nano-objects (Fig. 2) are atomic clusters, mineral and organic molecules, molecular agglomerates, particles and crystals, micro/nanofibers, liquid films and thin layers of the micro/nano scale dimensions. **Nanosciences** and **nanotechnologies** currently represent a rich field of ideas, experiments, theoretical considerations in materials sciences (**nanomaterials**), physics (**nanophysics**), fluids (**nanofluidics**), chemistry (**nanochemistry**), biology (**nanobiology**) and medicine (**nanomedicine**).

The physical phenomena at the micro/nanoscale are governed by conventional physical laws because the quantum are not dominating yet [1–3]. Nevertheless, there are differences in the behavior of the nano/micro and classical macrofluids due to the unique physical properties of micro/nanoparticles and their motion at the solid or soft walls. When we move from the macro- to micro- and nanoscale, the surface-to-volume ratio S/V becomes higher and the surface forces and surface phenomena become more important than the bulk forces and the motions produced by them. As particles decreases in size, a greater amount of them could be located at the surfaces. For instance (Fig. 3), when the diameter of the particle is d_0 = 0.5 nm typical for simple organic molecules, for the 2D(3D) spherical agglomerates with:

- d = 30 nm – almost ~5 % (0.1 %) are at the 2D(3D) surface;
- d = 10 nm – almost ~16 % (1 %) are at the 2D(3D) surface;
- d = 3 nm – almost ~52 % (10 %) are at the 2D(3D) surface.

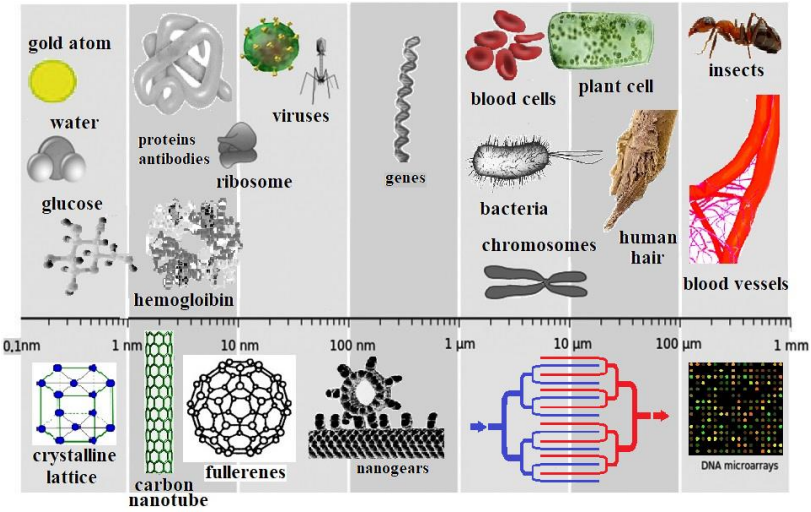

Fig. 2. Micro and nanoscale objects in nature and technique

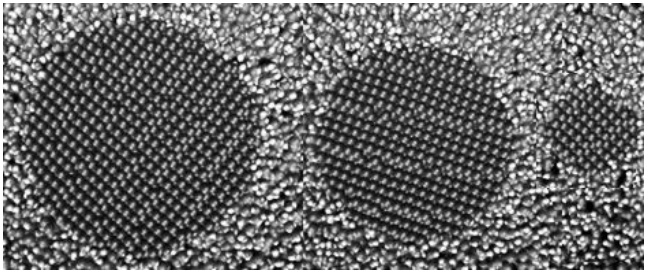

Fig. 3. Packing of micro/nanoparticles in 2D droplets

Therefore, at the nanoscale the S/V ratio becomes very high altering the mechanical, thermal and catalytic properties of materials, and promoting tremendous increase in their surface reactivity, adhesion, and other surface phenomena. Mechanical properties of nanosystems are of interest in the **nanomechanics** research; diffusion and reactions at nanoscale with fast ion transport are studied by **nanoionics**; rheological properties of nanofluids and solid materials are studied by **nanorheology**; friction at the nanoscale is studied by **nanotriboligy** [4]; propagation and reflection of visual light – by **nanooptics**, etc. Solution of the theoretical problems at the micro/nanoscale needs development of specific mathematical formulations of such mechanical, thermal and multiphysical problems.

1. FUNDAMENTALS OF MICROFLUIDICS AND NANOFLUIDICS

Numerous experiments with flows of micro and nano fluids through the microtubes, ducts and channels revealed that the measured pressures, velocites, volumetric flows and shear rates do not correspond to those values computed from classical Poiseuille and Couette flow solutions in the corresponding geometry with classical no-slip boundary conditions (BC) [1–3; 5; 6]. The most essential differences had been found in the flow patterns, pressure drops, shear stress and flow resistivity by the bigger influence of the wall roughness at the micro and nano scales [5; 6]. Therefore, reformulation of the BC problem is needed for better understanding of the differences between the flows of macroscopic fluids and micro/nano fluids.

Applicability of the slip boundary conditions have already been studied for the Newtonian fluid flows [6], macroscopic liquid flows near biological surfaces and interfaces [7], walls with special slide coating [8], penetrable walls [9], in polymer melts [10], and in turbulent flows with boundary slip [11].

The first formulation of the nonlinear slip BC has been proposed by Navier in 1873 in the form

$$(\hat{\mathrm{T}}\vec{\mathrm{n}})_\tau + \kappa \mathrm{v}_\tau = 0 \quad \text{on} \quad \partial\Omega, \tag{1}$$

Nanofluids as suspensions where $\partial\Omega$ is the boundary of the flow domain Ω, $\vec{\mathrm{v}}$ and $\hat{\mathrm{T}}$ are the fluid velocity and stress tensor, $\vec{\mathrm{n}}$ and $\vec{\tau}$ are normal and tangential unit vectors to the surface, κ is the 'friction' coefficient. Validity of the Navier BC for the fluid flows through rigid microtubes has been shown in [12].

Nanofluids as suspensions of nanoparticles and polymer molecules exhibit high thermal and electric conductivity, low specific heat, and unique electromagnetic properties due to high strength, thermal and electric conductivity of the nanoparticles and their magnetic properties [13]. Classical fluid dynamics and thermomechanical theories developed for the macroscopic systems are not fully applicable to the suspensions of nanoparticles as well as to uniform fluids at the micro and nano scales. Velocity slip, viscous dissipation, thermal creep and non-continuum effects like scattering at the wall, adhesion and changes in conformations must be taken into account [14–16] as well as electrokinetic phenomena [17]. For the solid nanoparticles in the concentrated (C > 5 %) nanofluids the shear-thickening behavior may also lead to the high pressure gradients for the steady fluid flow than those predicted by the Poiseuille law [18]. Gas microflows in MEMS and microfluidic devices can be used for extracting biological samples, cooling integrated circuits and active control over the aerodynamic forces [19; 20].

The first experimental study conducted for the gas flow in the rectangular glass channels with hydraulic radius $\mathrm{D_h}$ = 45.5–83.1 μm and silicon channels with $\mathrm{D_h}$ = 55.8–72.4 μm of microminiature Joule–Thomson refrigerators revealed the friction coefficient about 10–30 % higher in silica channels and in 3–5 times high in glass channels than those predicted by the Moody chart for the friction factor against

the Reynolds number at different relative roughness ε / D_h, where ε is the roughness height [21]. In the micro and nano channels due to the tremendous increase in the surface-to-volume ratio the relative roughness becomes the most influencing factor, which has to be taken into account in the BC via complex geometry of the wall with roughness, as well as complex interaction of the flow and nanoparticles with the wall.

Experimental study of the fluid flow (1-, 2-propanol and 1-, 3-pentanol) through silicon microchannels with D_h = 5; 12; 25 μm also demonstrated an increase in the friction coefficient by 5–30 % depending on the temperature within the limits $T = 0 - 85^{\circ}C$ compared to the classical computations on the Navier-Stokes equations with no-slip boundary conditions [22]. Water flow through rectangular stainless steel microchannels with D_h = 133–367 μm and width to height ratios W/H = 0.333–1 has been studied in [23]. The friction factors for both laminar and turbulent flows have been found deviated from the classical predictions, and the geometry factor W/H was found to have important effects on the flow. The laminar to turbulence transition occurred at the critical Reynolds numbers Re^* = 200–700 depending on D_h and W/H. The value Re^* becomes lower as the size of the microchannel decreases. Water flow through the stainless steel and fused silica circular microtubes with diameters D = 50–254 μm and ε / D = 0.69–3.5 % at Re = 100–2000 also exhibited higher friction than those predicted by the classical fluid dynamics [15]. The difference increased with the decreasing D and increasing Re values. The flow transition has been observed at Re^* = 300-900 depending on the microtube diameter D = 50–150 μm. For the fluid flows in rectangular metallic channels with widths W = 150–600 μm and heights H = 22.7–26.3 μm an approximate 20 % increase over the classical theory prediction in the friction factor at low H/W ratios has been revealed [24]. The water flow through trapezoidal silicon microchannels with D_h = 51.3–168.9 μm and ε / D = 1.76–2.85 % at Re < 1500 demonstrated the friction factor by 8–38 % higher than the classical theory prediction for laminar flows [25].

A good review of literature published between 1983 and 2005 on the experimental studies of the friction coefficient and laminar to turbulence transition Re^* values in the microchannels and tubes of different geometry and materials is given in [16]. It is shown when ε / D_h < 1 %, the classical computations for the corresponding Poiseuille and Couette laminar flows remain valid. A positive deviation of the friction factor from the conventional theory is observed due to the high roughness and compressibility effects. For instance, smaller friction factors detected in gas flows through fused silica microtubes with D = 10–20 μm are produced by rarefaction effect.

The results of the abovementioned experimental studies confirmed that the flow resistances are about 10–90 % higher than the theoretical values for the corresponding geometry and material parameters, and some of them even by 350 % over the theoretical predictions [16; 21; 26].

Flows of the micro/nanofluids are governed by the Navier–Stokes equations [1–3]:

$$\frac{d\rho_{eff}}{dt} + \rho_{eff}\,\mathrm{div}(\vec{v}) = 0, \tag{2}$$

$$\rho_{eff}\left(\frac{\partial\vec{v}}{\partial t} + (\vec{v}\cdot\nabla)\vec{v}\right) = -\nabla p + \mu_{eff}\,\Delta\vec{v} + \rho_{eff}\,\vec{f}, \tag{3}$$

$$\rho_{eff}\,c_{eff}\,\frac{dT}{dt} = \mathrm{div}(\lambda_{eff}\nabla T) + \mu_{eff}\left(\frac{\partial v_i}{\partial x_k} + \frac{\partial v_k}{\partial x_i} - \frac{\delta_{ik}}{3}\frac{\partial v_k}{\partial x_k}\right)^2 + \zeta_{eff}\left(\frac{\partial v_k}{\partial x_k}\right)^2, \tag{4}$$

where $\vec{v}$ and p – are the flow velocity and hydrostatic pressure; ρ_{eff}, μ_{eff}, ζ_{eff}, c_{eff} and λ_{eff} are the density, dynamic and second viscosity, heat conductivity and heat capacity of the fluid which are actually temperature dependent functions; $\vec{f}$ is the volume density of external forces; T is the temperature; δ_{ik} is the unit tensor. In the case of incompressible fluids ρ_{eff} = const and the first term in (2) disappears; $\mathrm{div}(\vec{v}) = 0$ and two last terms in (4) disappear.

The effective density of the micro/nanofluds can be introduced in a usual form accepted for mixtures [27]

$$\rho_{eff} = \rho_p C + \rho_{bf}(1-C), \tag{5}$$

where ρ_p and ρ_{bf} are densities of particles and basic fluid, C is concentration of particles.

The expressions for the effective heat conductivity k_{eff} and specific heat c_{eff} of the micro/nanofluids have been derived in the form [28]

$$k_{eff} = k_{bf}\,\frac{(k_p + 2k_{bf}) - 2C(k_{bf} - k_p)}{(k_p + 2k_{bf}) + C(k_{bf} - k_p)} + k_{Brownian},$$
$$k_{Brownian} = 5\cdot 10^4\,\beta C\rho_{bf}\,c_{bf}\sqrt{\frac{k_B T}{d_p}}\,f(T,C), \tag{6}$$

$$c_{eff} = \frac{\rho_p c_p C + \rho_{bf} c_{bf}(1-C)}{\rho_p C + \rho_{bf}(1-C)}, \tag{7}$$

where k_p, k_{bf} and c_p, c_{bf} are heat conductivity and specific heat of the particles and base fluid, k_B is the Boltzmann constant, β is the constant that depends on the temperature, material and concentration of the particles, $f = f(T,C)$ is the function that has to be determined from experiments.

The heat capacity is well defined by the mixture models [27]

$$c_{eff} = c_p C + c_{bf}(1-C). \tag{8}$$

The viscosity of the micro/nanofluids as well as in the suspensions of macroscopic particles is a very complex value, and there are many different formulas for μ_{eff}. Among the most popular ones are:

1) the non-constant so-called roughness viscosity $\mu_{\text{eff}}(\text{r})$ [29]

$$\mu_{\text{eff}}(\text{r}) = \text{A}\mu_{\text{bf}}\,\text{Re}_{\varepsilon}\frac{\text{r}}{\varepsilon}\left(1-\exp\left(\frac{\text{Re}_{\varepsilon}}{\text{Re}}\frac{\text{r}}{\varepsilon}\right)\right)^2, \tag{9}$$

where r is the radial coordinate, $\text{Re} = \rho_{\text{eff}}\,\text{v}^*\text{d}/\mu_{\text{eff}}$, $\text{Re}_{\varepsilon} = \rho_{\text{eff}}\,\text{U}\varepsilon/\mu_{\text{eff}}$, d is the characteristic diameter of the channel, v* is the average flow velocity, U is the velocity at the top of the roughness element, A is the material-dependent constant;
2) constant viscosity model [30]

$$\mu_{\text{eff}} = \frac{\mu_{\text{bf}}}{1-\alpha(\text{d}_{\text{p}}/\text{d}_{\text{f}})^{-0.3}\text{C}^{1.03}}, \tag{10}$$

where $\text{d}_{\text{f}} = \left(6\text{M}_{\text{bf}}/\pi\text{N}_{\text{A}}\rho_{\text{bf}}\right)^{1/3}$ is the base fluid equivalent diameter, d_{p} is the diameter of the micro/nanoparticles, M_{bf} is the molecular weight of the base fluid, N_{A} is the Avogadro number;
3) Kn-dependent viscosity [5]

$$\mu_{\text{eff}} = \frac{\mu_{\text{bf}}}{1+\alpha\text{Kn}}, \alpha = \frac{2\alpha_0}{\pi\tan(\alpha_1\text{Kn}^{\beta})}, \tag{11}$$

where $\alpha = 0.4$, $\alpha_0 = 64/3\pi(1-4/\text{b})$, $\alpha_1 = 4$, $\beta = -1$ [34];
4) general approximation for the concentrated suspensions

$$\mu_{\text{eff}} = \mu_{\text{bf}}(1+\text{k}_1\text{C}+\text{k}_2\text{C}^2), \tag{12}$$

where, for instance, $\text{k}_1 = 39.1, \text{k}_2 = 533.9$ values for Al/water nanofluid [31].

When the fluid flow is studied at the isothermal conditions, the BC for (1)–(2) in the most general form are [1–6]

$$\left(\text{v}-\text{v}_{\text{w}}-\text{C}_1\text{Kn}\frac{\partial\text{v}}{\partial\text{n}}+\text{C}_2\text{Kn}^2\frac{\partial^2\text{v}}{\partial\text{n}^2}\right)\Bigg|_{\partial\Omega} = 0, \tag{13}$$

where v_{w} is the velocity of the moving wall, $\text{Kn} = \lambda/\text{L}$ is the Knudsen number, λ is the mean free path of the particles in the suspension, L is the characteristic length, C_1 and C_2 are fluid-specific constants that must be determined from experiments with the fluid under consideration.

The layer produced by the particles scattered by the rough wall is called Knudsen layer. Its thickness was evaluated in the discrete hard sphere model and in the continuous model of a fluid accordingly as [5]

$$\delta = \frac{\text{k}_{\text{B}}\text{T}}{\pi\text{d}_{\text{p}}^2\text{p}}, \quad \delta = \mu_{\text{eff}}\sqrt{\frac{\pi}{2\text{p}\rho_{\text{eff}}}}.$$

From the theoretical considerations the coefficient $\text{C}_1 = (2-\sigma)/\sigma$, where σ is the tangential momentum accommodation factor; $\sigma = 1$ for purely diffuse reflection and $|\sigma| < 1$ for mixed reflection [14]. The term C_1Kn in (13) is the

constant slip length of the particles at the rough wall due to diffusive reflection [19]. A good review on the experimental data of the coefficients $C_{1,2}$ for different micro/nanofluids is given in [5, p. 74]. Summarizing the table presented there, one can accept $C_1 \in [1;1.15]$, $C_2 \in [0.5;1.31]$ for numerical computations.

There are also a series of modifications of (11) for specified fluids like [5]

$$\left(\mathrm{v} - \mathrm{v_w} - \frac{2-\sigma}{\sigma} \frac{\mathrm{Kn}}{1-\mathrm{Kn}\cdot \mathrm{f(Kn)}} \frac{\partial \mathrm{v}}{\partial \mathrm{n}} \right)\Bigg|_{\partial\Omega} = 0, \tag{14}$$

where $\mathrm{f(Kn)}$ is an empirical parameter that must be determined from experiments, $|\mathrm{f(Kn)}|<1$, or for compressible fluids [35; 36]

$$\left(\mathrm{v} - \mathrm{v_w} - \frac{\mu_{\mathrm{eff}}}{\rho_{\mathrm{eff}}} \frac{\partial}{\partial \tau} \ln \rho_{\mathrm{eff}} \right)\Bigg|_{\partial\Omega} = 0. \tag{15}$$

Molecular dynamics simulations revealed that the velocity slip at the wall decreases with increase of the ratio ε / λ for both regular and stochastic roughness [32]. In the transition regime $\mathrm{Kn} > 0.1$ the constitutive laws for the stress tensor, heat flux vector and other parameters break down requiring higher-order correcting terms [33].

Therefore the value ε / λ can be considered as a criterion for the no-slip boundary conditions acceptance. When $\varepsilon \le \lambda$ the no-slip condition is satisfied, otherwise significant slip at the wall is present. As it was shown by comparative numerical simulations of the micro- and nanochannel flows in different geometries conducted by molecular dynamics simulations, numerical solutions of the Boltzmann equation as well as direct computations on the Navier-Stokes equations, the slip-flow approach is remarkably robust in the meaning that it is qualitatively accurate and physically relevant [19].

Therefore, three different cases can be distinguished [1–6]:

1) $\mathrm{Kn} < 0.01$: the no-slip BC $\mathrm{v}|_{\partial\Omega} = 0$ is satisfied;
2) $0.01 < \mathrm{Kn} \le 0.1$: the first-order slip BC (11) with $C_2 = 0$ (microfluids);
3) $0.1 < \mathrm{Kn} \le 1$: the second-order slip DC (11) with $C_2 \ne 0$ (nanofluids).

When the coupled heat and mass transfer equations (1)–(3) are studied, the Navier–Stokes and heat balance equations are solved with the modified second order boundary conditions in the form:

$$\begin{gathered} \left(\mathrm{v} - \mathrm{v_w} - \frac{2-\sigma}{\sigma} \mathrm{Kn} \frac{\partial \mathrm{v}}{\partial \mathrm{n}} - \frac{3(\gamma-1)}{2\pi\gamma} \frac{\mathrm{Kn}^2\,\mathrm{Re}}{\mathrm{Ec}} \frac{\partial \mathrm{T}}{\partial \tau} \right)\Bigg|_{\partial\Omega} = 0, \\ \left(\mathrm{T} - \mathrm{T_w} - \frac{2\gamma(2-\tilde{\sigma})}{(\gamma+1)\tilde{\sigma}} \frac{\mathrm{Kn}}{\mathrm{Pr}} \frac{\partial \mathrm{T}}{\partial \mathrm{n}} \right)\Bigg|_{\partial\Omega} = 0, \end{gathered} \tag{16}$$

where T and $\mathrm{T_w}$ are the temperatures in the flow and at the wall, τ is the tangential direction (coordinate), $\tilde{\sigma}$ is the energy accommodation coefficient, $\gamma = \mathrm{C_p} / \mathrm{C_V}$ is

the ratio of the specific heats at constant pressure and volume of the suspension respectively, $\mathrm{Re}=\rho_{\mathrm{eff}}\,\mathrm{v}^{*}\mathrm{d}/\mu_{\mathrm{eff}}$ is the Reynolds number, $\mathrm{Pr}=\mathrm{c}_{\mathrm{eff}}\,\mu_{\mathrm{eff}}/\lambda_{\mathrm{eff}}$ is the Prandtl number, $\mathrm{Ec}=(\mathrm{v}^{*})^{2}/\mathrm{c}_{\mathrm{eff}}\,\Delta\mathrm{T}$ is the Eckert number, $\Delta\mathrm{T}$ is the specified temperature difference in the domain; perfect energy exchange corresponds to $\tilde{\sigma}=1$ when the energy of the reflected (scattered) particles matches the wall temperature (no temperature jump).

Thermal and tangential momentum accommodation coefficients have been measured for different typical gases and surfaces, and they were shown to be strongly dependent on the material and surface state [5]. Their values can be reduced by applying suitable surface preparation techniques.

The solutions of classical laminar pressure-driven (Poiseuille) and shear-driven (Couette) channel flows of incompressible Newtonian liquids have been generalized for the velocity slip BC, and the corresponding analytical solutions have been obtained and compared to the experimental data [5; 19; 37]. In this textbook the generalized solutions at the isothermal conditions are given and some more problems for individual tasks are proposed. Actual flows of suspensions of micro or/and nanoparticles are much more complex and the solutions of corresponding systems of equations have no analytical or semi-analytical solutions. In such cases the solutions must be found out by numerical computations in complex expansions, with finite difference method, finite element, discrete particle dynamics method, Lattice–Boltzmann method and other numerical schemes. In each case the corresponding analytical solution for checking and final validation of the numerical scheme is needed. All known analytical and semi-analytical solutions for the channel flows are considered in this textbook.

2. COUETTE FLOWS IN TUBES AND CHANNELS

2.1. Laminar flow between two parallel plates

2.1.1. Classical fluids

The Couette flows are generated by moving wall(s) of the channel(s) without any pressure gradient applied. The simplest examples are flows between two parallel plates generated by the motion of one or both plates at different velocities (Fig. 4a); flows between two coaxial cylinders rotating with different angular velocity (Fig. 4b). In both cases the approximation is valid when the distance between the surfaces is relatively small, i. e. $\mathrm{h} << \mathrm{L}$ (Fig. 4a), $\mathrm{R}_2-\mathrm{R}_1 << \mathrm{R}_1$ (Fig. 4b), where L is the length of the plates.

In the laminar flows the velocity vector has only one component, i. e. the flow is one-dimensional (1D). In the flow between the parallel plates one has $\vec{\mathrm{v}}=(\mathrm{v}_{\mathrm{x}},\mathrm{v}_{\mathrm{y}},\mathrm{v}_{\mathrm{z}})=(\mathrm{v},0,0)$ in the Cartesian coordinate system combined with geometry according to Fig.4a. Let's assume the flow is stationary and $\partial/\partial\mathrm{t}=0$ in (3). Let's

also suggest the width of the plates W is large enough (W>>h) so one may assume $\partial/\partial z = 0$ in (1)–(2). The mass forces are absent and the flow is driven only by the motions of the plates with constant velocities V_1 and V_2. For distinctness let's assume $V_1 > V_2$ (Fig.4a). Then the equation (2) gives $\partial v / \partial x = 0$. Since $\partial v/\partial z = 0$ also, it gives $v = v(y)$.

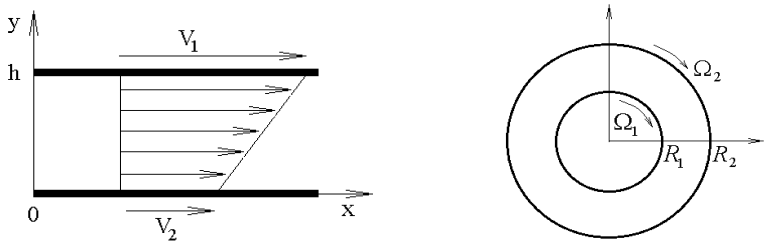

a *b*

Fig. 4. Laminar flows between parallel plates (a) and coaxial cylinders (b)

It is easy the check that in this case the second term in the left-hand side of (3) will be

$$(\vec{v},\nabla)\vec{v} = \left(v_x \frac{\partial}{\partial x} + v_y \frac{\partial}{\partial y} + v_z \frac{\partial}{\partial z} \right) \begin{pmatrix} v_x \\ v_y \\ v_z \end{pmatrix} = v_x(y) \frac{\partial}{\partial x} \begin{pmatrix} v_x(y) \\ 0 \\ 0 \end{pmatrix} = \begin{pmatrix} 0 \\ 0 \\ 0 \end{pmatrix}.$$

Then the projection of the vectorial equation (3) onto the axis 0y gives $\partial p / \partial y = 0$ that means $p = p(x)$ because $\partial p/\partial z = 0$. The projection of (3) onto the axis 0x gives

$$\frac{dp(x)}{dx} = \mu \frac{d^2 v(y)}{dy^2} \quad . \tag{17}$$

In (17) and following equations the subscripts 'eff' are omitted for brevity. In the left-hand side of (17) we have a function depending on x only, while in the right-hand side of (17) the function depends on y only, and the both functions are equal to each other at any time and in any point of space. It implies that both functions are constant. The condition $\frac{dp(x)}{dx} \equiv k = \text{const}$ with the inlet and outlet BC $p\big|_{x=0,L} = 0$ gives $k = 0$. Then integration of (17) gives

$$v(y) = C_1 + C_2 y \,. \tag{18}$$

The BC (13) for classical fluids ($C_{1,2} = 0$) are $v(0) = V_2$, $v(h) = V_1$ that gives the solution (18) in the form [38]

$$v(y) = V_1 - \frac{V_1 - V_2}{h} y \,. \tag{19}$$

Integration of (19) over the cross-sectional area gives the following expression for the volumetric flow rate

$$Q_{\text{Couette}} = W\int_0^h v(y)dy = \frac{(V_1 + V_2)hW}{2}. \quad (20)$$

The shear stress in the fluid is constant over the cross section

$$\tau_{\text{Couette}} \equiv \mu\frac{dv}{dy} = -\mu\frac{V_1 - V_2}{h}. \quad (21)$$

The velocity field is presented in Fig.4a, while the shear stress is constant.

2.1.2. Micro/nanofluids

The flow is governed by the same equations (2)-(3) and the flow solution is given by (18). The BC (13) have the form

$$\begin{aligned} y = 0: \quad & v = V_2 - \alpha_1\frac{\partial v}{\partial y} - \beta_1\frac{\partial^2 v}{\partial y^2} \\ y = h: \quad & v = V_1 + \alpha_2\frac{\partial v}{\partial y} - \beta_2\frac{\partial^2 v}{\partial y^2} \end{aligned}, \quad (22)$$

with different roughness parameters $\alpha_1 = C_{11}Kn$ and $\alpha_2 = C_{12}Kn$, $\beta_1 = C_{21}Kn^2$ and $\beta_2 = C_{22}Kn^2$ on two plates, for generalization purposes. The changed sign before α_1 is because of the differences of the directions of the derivative $\partial v/\partial y$ and the scatter of the particles.

Substitution of (18) into (22) gives the velocity distribution

$$v(y) = \frac{V_1 h + \alpha_2 V_1 + \alpha_1 V_2}{h + \alpha_2 + \alpha_1} - \frac{V_1 - V_2}{h + \alpha_2 + \alpha_1}y. \quad (23)$$

When $\alpha_{1,2} = 0$, $\beta_{1,2} = 0$ the expression (23) is transformed into (19).

Integration of (23) over the cross section of the channel gives

$$Q_{\text{Couete slip}} = W\int_0^h v(y)dy = W\frac{(V_1 + V_2)h^2 + 2h(\alpha_2 V_1 + \alpha_1 V_2)}{2(h + \alpha_2 + \alpha_1)}, \quad (24)$$

and the shear stress is

$$\tau_{\text{Couete slip}} = -\mu\frac{V_1 - V_2}{h + \alpha_2 + \alpha_1}. \quad (25)$$

The difference between the flow rates

$$Q_{\text{Couete slip}} - Q_{\text{Couete}} = Wh\frac{(\alpha_2 - \alpha_1)(V_1 - V_2)}{2(h + \alpha_2 + \alpha_1)} \quad (26)$$

could be negative or positive depending on the properties of the plates, namely

$$\begin{aligned} Q_{\text{Couete slip}} - Q_{\text{Couete}} > 0, \text{ if } \alpha_2 > \alpha_1, \\ Q_{\text{Couete slip}} - Q_{\text{Couete}} < 0, \text{ if } \alpha_2 < \alpha_1. \end{aligned} \quad (27)$$

When $V_1 < V_2$, the relationships between Q_{Couete} and $Q_{\text{Couete slip}}$ are inverse to (27). The difference between the shear stresses

$$\tau_{\text{Couete slip}} - \tau_{\text{Couete}} = \frac{\mu(V_1 - V_2)(\alpha_2 + \alpha_1)}{h(h + \alpha_2 + \alpha_1)} > 0 \qquad (28)$$

and the shear stress in the slip flow is always lower by the absolute value that the shear stress in the no-slip flow.

Therefore, by using the plates with different first order roughness coefficients α_1 and α_2 we can obtain the Couette flows with higher/lower volumetric rate at the same shear stress at the walls that can be beneficial for different microfluidic applications. Since the flow field is linear, the second derivatives in (13) have no influence of the flow parameters. It means, the Couette flow behaviour is the same for both microfluids and nanofluids.

2.2. Laminar flow between two coaxial rotating cylinders

2.2.1. Classical fluids

Two coaxial cylinders with axis 0z and radiuses R_1 and R_2 rotate with the angular velocity Ω_1 and Ω_2 (let's assume $\Omega_2 > \Omega_1$) are considered (Fig.4b). The 1D velocity vector is $\vec{v} = (v_r, v_\theta, v_z) = (0, v, 0)$. The flow is steady ($\partial/\partial t = 0$) and the length of the cylinders is big enough such as $\partial/\partial z = 0$. The flow is axisymmetric and $\partial v / \partial\theta = 0$. Then from (2) we have $v = v(r)$. Substitution into the second term in the left-hand side of eq. (3) gives

$$(\vec{v}, \nabla)\vec{v} = \left(v_r \frac{\partial}{\partial r} + \frac{v_\theta}{r} \frac{\partial}{\partial \theta} + v_z \frac{\partial}{\partial z} \right) \begin{pmatrix} v_r \\ v_\theta \\ v_z \end{pmatrix} = \frac{v_\theta}{r} \frac{\partial}{\partial \theta} \begin{pmatrix} 0 \\ v_\theta(r) \\ 0 \end{pmatrix} = 0 .$$

Projection of (3) onto the axis 0r gives the same condition for the pressure drop ($dp(x)/dx = 0$) and the projection onto the axis 0θ gives the ordinary differential equation

$$\frac{1}{r} \frac{\partial}{\partial r} \left(r \frac{\partial v(r)}{\partial r} \right) - \frac{v(r)}{r^2} = 0 . \qquad (29)$$

Solution of (29) is

$$v = C_1 r + C_2 \frac{1}{r} . \qquad (30)$$

The coefficients $C_{1,2}$ can be found from the no-slip BC $v(R_1) = \Omega_1 R_1$, $v(R_2) = \Omega_2 R_2$ and the final expression is [38]

$$v(r) = \frac{\Omega_2 R_2^2 - \Omega_1 R_1^2}{R_2^2 - R_1^2} r - \frac{(\Omega_2 - \Omega_1) R_1^2 R_2^2}{R_2^2 - R_1^2} \frac{1}{r} . \qquad (31)$$

Integration of (31) over the cross section of the channel gives the flow rate

$$Q_{\text{Couette}} = \frac{2\pi W}{3(R_2^2 - R_1^2)} \left((\Omega_2 R_2^2 - \Omega_1 R_1^2)(R_2^2 + R_2 R_1 + R_1^2) - 3(\Omega_2 - \Omega_1) R_1^2 R_2^2 \right), \qquad (32)$$

and the shear stress is

$$|\tau_{\text{Couette}}| = \mu_{\text{eff}}\left(\frac{\Omega_2 R_2^2 - \Omega_1 R_1^2}{R_2^2 - R_1^2} + \frac{(\Omega_2 - \Omega_1) R_1^2 R_2^2}{R_2^2 - R_1^2}\frac{1}{r^2}\right). \tag{33}$$

In the non-dimensional form (31)-(33) can be written as

$$v^\circ(\wp) = \left(\frac{\Omega R^2 - 1}{R^2 - 1}\wp - \frac{(\Omega - 1)R^2}{R^2 - 1}\frac{1}{\wp}\right). \tag{34}$$

$$Q^\circ = \frac{2\left((\Omega R^2 - 1)(R^2 + R + 1) - 3(\Omega - 1)R^2\right)}{3(R^2 - 1)}, \tag{35}$$

$$|\tau^\circ| = \frac{\Omega R^2 - 1}{R^2 - 1} + \frac{(\Omega - 1)R^2}{R^2 - 1}\frac{1}{\wp^2}, \tag{36}$$

where $v^\circ = v/\Omega_1 R_1$, $\wp = r/R_1$, $\Omega = \Omega_2/\Omega_1 > 1$, $R = R_2/R_1 > 1$, $Q^\circ = Q/(\pi\Omega_1 R_1^2 W)$, $\tau^\circ = \tau/\mu_{\text{eff}}\Omega_1$.

The dependencies (34)–(36) are presented in Fig. 5a–c for some values of Ω and R.

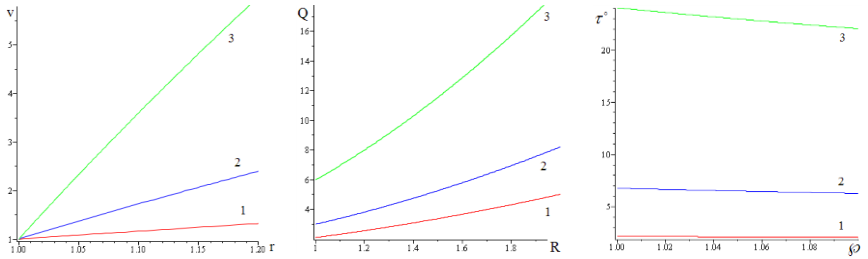

a *b* *c*

Fig. 5. Non-dimensional dependencies $v^\circ(\wp)$ *(a),* $Q^\circ(R)$ *(b),* $\tau^\circ(\wp)$ *(c) for the no-slip flow at different values* Ω *=1.1; 2; 5 – curves 1,2,3 accordingly*

2.2.2. Micro/nanofluids

The flow is governed by the same equations (2)-(3) and the flow solution is given by (30). The BC (13) have the form

$$r = R_1 : v = \Omega_1 R_1 + \alpha_1\frac{\partial v}{\partial r} - \beta_1\frac{\partial^2 v}{\partial r^2}, \quad r = R_2 : v = \Omega_2 R_2 + \alpha_2\frac{\partial v}{\partial r} - \beta_2\frac{\partial^2 v}{\partial r^2}. \tag{37}$$

Substitution of (30) into (37) gives the velocity distribution

$$v_{\text{Couette}}^{\text{slip}}(r) = \frac{\Omega_2 R_2^4 A_1 - \Omega_1 R_1^4 A_2}{R_2^3(R_2 - \alpha_2)A_1 - R_1^3(R_1 - \alpha_1)A_2}r - \frac{\Omega_2 R_1^3 R_2^4(R_1 - \alpha_1) - \Omega_1 R_1^4 R_2^3(R_2 - \alpha_2)}{R_2^3(R_2 - \alpha_2)A_1 - R_1^3(R_1 - \alpha_1)A_2}\frac{1}{r}, \tag{38}$$

where $A_{1,2} = R_{1,2}^2 + \alpha_{1,2}R_{1,2} - \beta_{1,2}$.

Integration of (38) over the cross section of the channel gives the flow rate

$$Q_{Couette}^{slip} = \frac{2\pi W(R_2 - R_1)}{3(R_2^3(R_2-\alpha_2)A_1 - R_1^3(R_1-\alpha_1)A_2)}\Big((\Omega_2 R_2^4 A_1 - \Omega_1 R_1^4 A_2)\times \\ \times(R_2^2 + R_1R_2 + R_1^2) - 3(\Omega_2 R_1^3 R_2^4(R_1-\alpha_1) - \Omega_1 R_1^4 R_2^3(R_2-\alpha_2))\Big). \quad (39)$$

The shear stress in the flow is

$$\tau_{Couette}^{slip}(r) = \mu_{eff}\left(\frac{\Omega_2 R_2^4 A_1 - \Omega_1 R_1^4 A_2}{R_2^3(R_2-\alpha_2)A_1 - R_1^3(R_1-\alpha_1)A_2} + \right. \\ \left. + \frac{\Omega_2 R_1^3 R_2^4(R_1-\alpha_1) - \Omega_1 R_1^4 R_2^3(R_2-\alpha_2)}{R_2^3(R_2-\alpha_2)A_1 - R_1^3(R_1-\alpha_1)A_2}\frac{1}{r^2}\right). \quad (40)$$

In the non-dimensional form (38)-(40) can be re-written as

$$v^\circ(r) = \frac{\Omega R^4 A_1 - A_2}{R^3(R-\tilde\alpha_2)A_1 - (1-\tilde\alpha_1)A_2}\wp - R^3\frac{\Omega R(1-\tilde\alpha_1) - (R-\tilde\alpha_2)}{R^3(R-\tilde\alpha_2)\tilde A_1 - (1-\tilde\alpha_1)\tilde A_2}\frac{1}{\wp}, \quad (41)$$

$$Q^\circ = \frac{2(R-1)\Big((\Omega R^4\tilde A_1 - \tilde A_2)(R^2+R+1) - 3(\Omega R^4(1-\tilde\alpha_1) - R^3(R-\tilde\alpha_2))\Big)}{3(R^3(R-\tilde\alpha_2)\tilde A_1 - (1-\tilde\alpha_1)\tilde A_2)}, \quad (42)$$

$$\tau^\circ(r) = \frac{\Omega R^4\tilde A_1 - \tilde A_2}{R^3(R-\tilde\alpha_2)\tilde A_1 - (1-\tilde\alpha_1)\tilde A_2} + \frac{\Omega R^4(1-\tilde\alpha_1) - R^3(R-\tilde\alpha_2)}{R^3(R-\tilde\alpha_2)\tilde A_1 - (1-\tilde\alpha_1)\tilde A_2}\frac{1}{\wp^2}, \quad (43)$$

where $\tilde A_1 = 1+\tilde\alpha_1 - \tilde\beta_1$, $\tilde A_2 = R^2 + \tilde\alpha_2 R - \tilde\beta_2$, $\tilde\alpha_{1,2} = \alpha_{1,2}/R_1$, $\tilde\beta_{1,2} = \beta_{1,2}/R_1^2$.

The dependencies (41)-(43) for some values $\tilde\alpha_{1,2}$ and $\tilde\beta_{1,2}$, and for the same values of Ω and R as were used in Fig.5a–c are presented in Fig. 6a–c.

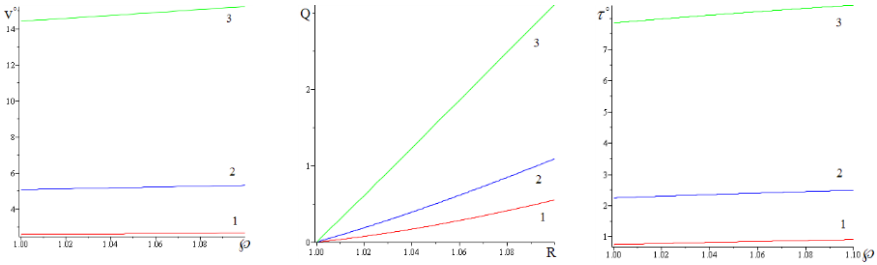

a b c

Fig. 6. Non-dimensional dependencies $v^\circ(\wp)$ *(a),* $Q^\circ(R)$ *(b),* $\tau^\circ(\wp)$ *(c) for the slip flow at* $\tilde\alpha_1 = 1.5$, $\tilde\alpha_2 = 1.3$, $\tilde\beta_1 = 0.5$, $\tilde\beta_2 = 0.3$ *and different values* Ω *=1.1; 2; 5 – curves 1,2,3 accordingly*

Individual task 1: Using (34)–(36) and (41)–(43) estimate the ranges for the roughness parameters $\tilde\alpha_{1,2}$, $\tilde\beta_{1,2}$ when the flow rate could be increased and the shear

stress could be decreased in the micro/nanoflows in comparison to the classical fluids, in the same way like it was done in (26)–(28) for the Couette flow between two parallel plates.

3. LAMINAR FLOW IN AN INCLINED DUCT

3.1. Classical fluids

Laminar $\vec{v} = (v_x, 0, 0)$ flow of an incompressible Newtonian fluid in a rectangular cuvette $\{x \in [0, L] \times y \in [0, h] \times z \in [0, W]\}$, h/W<<1 inclined to the horizon by the angle φ (Fig. 7) is considered. The flow is governed by the force of gravity. The system of coordinates is connected with bottom of the cuvette.

The incompressibility condition (2) gives again $v_x = v(y)$. Check that in this case $(\vec{v}, \nabla)\vec{v} = 0$. The projection of the momentum equation (3) onto the axis 0y is

$$\mu \frac{d^2 v}{dy^2} + \rho g \sin\varphi = 0 \ . \qquad (44)$$

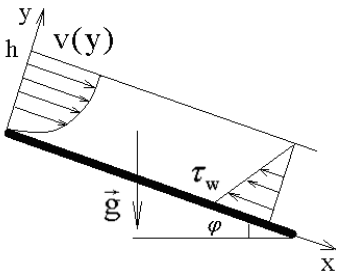

Fig. 7. Schema of the laminar flow in an inclined duct

Intergation of (44) with the velocity no-slip BC and the bottom and the free surface kinematic BC at the open surface of the cuvette

$$v(y)\big|_{y=0} = 0, \quad \left.\frac{dv(y)}{dy}\right|_{y=h} = 0 . \qquad (45)$$

gives the velocity profile, flow rate and shear stress distributions respectively

$$v_{incl}(y) = \frac{\rho g \sin\varphi}{2\mu_{eff}} y(2h - y),$$

$$Q_{incl} = \frac{W\rho g \sin\varphi}{3\mu_{eff}} h^3, \qquad (46)$$

$$\tau_{incl} = \rho g \sin\varphi \cdot (h - y) = \tau_b \left(1 - \frac{y}{h}\right),$$

where $\tau_b = \rho g h \sin\varphi$ is the shear stress at the bottom of the duct. The velocity and shear stress profiles and plotted in Fig. 3.

3.2. Micro/nanofluids

Integration of the same equation (44) with the velocity slip BC (13) at the bottom and free surface kinematic BC (45) gives:

$$v_{incl}^{slip}(y)=\frac{\rho g\sin\varphi}{2\mu_{eff}}\big(2(\alpha h+\beta)+y(2h-y)\big),$$

$$Q_{incl}^{slip}=\frac{W\rho g\sin\varphi}{\mu_{eff}}h(\alpha h+\beta+\frac{h^2}{3}), \qquad (47)$$

$$\tau_{incl}^{slip}=\tau_b\left(1-\frac{y}{h}\right),$$

where α,β are the roughness coefficients at the bottom.

Note that in this flow the velocity profile and flow rate in the nanofluids and microfluids will be different because the coefficient β is present in their expressions (47), while the distributions of shear stresses are the same in both cases.

Comparing (47) and (46), one may conclude that

$$v_{incl}^{slip}(0)=\frac{\rho g\sin\varphi}{\mu}(\alpha h+\beta)>0,$$

$$v_{incl}^{slip}(h)-v_{incl}(h)=\frac{\rho g\sin\varphi}{\mu}\big(\alpha h+\beta\big)>0, \qquad (48)$$

$$Q_{incl}^{slip}-Q_{incl}=\frac{W\rho g\sin\varphi}{\mu_{eff}}h(\alpha h+\beta)>0,$$

$$\tau_{incl}^{slip}=\tau_{incl}$$

for positive α,β values. Since the negative β coefficients have also been reported [5], the comparative results are valid for the cases with $\alpha h+\beta>0$.

4. POISEUILLE FLOWS IN TUBES AND CHANNELS

4.1. Laminar flow between two parallel plates

4.1.1. Classical fluids

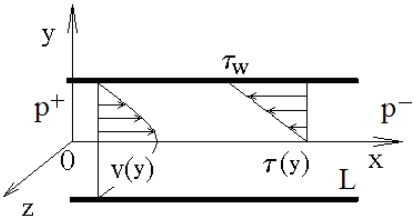

Fig. 8. Poiseuille flow between the parallel plates

Poiseuille flows are governed by the pressure drop $\Delta p=p^+-p^-$ applied between the inlet $p|_{x=0}=p^+$ and outlet $p|_{x=L}=p^-$ of the channel. In the considered case the channel is built by two parallel plates (Fig. 8) of dimensions $L\times W$ with a small distance $h<<\min\{L,W\}$ between them.

The same conclusions can be derived from (2)–(3), namely:

1) $v_x = v(y)$;

2) $p = p(x)$, $\dfrac{dp}{dx} = \text{const} = -\dfrac{\Delta p}{L}$.

Integrating the projection of the momentum equation onto the axis 0x

$$\mu_{\text{eff}} \frac{d^2 v}{dy^2} = \frac{\Delta p}{L} \tag{49}$$

one can obtain

$$v(y) = C_2 + C_1 y - \frac{\Delta p}{2\mu L} y^2 . \tag{50}$$

The constants $C_{1,2}$ can be found from the velocity no-slip at the wall and symmetric profile at the axis BCs. Finally

$$v_{\text{paral}}(y) = \frac{\Delta p h^2}{2\mu L}\left(h^2 - y^2\right), \qquad p(x) = p^+ - \frac{\Delta p}{L} x. \tag{51}$$

Integration of the velocity over the cross-section of the channel gives the volumetric flow rate

$$Q_{\text{paral}} = \frac{2}{3}\frac{\Delta p W h^3}{\mu L} \quad . \tag{52}$$

Then the hydraulic resistivity of the channel $Z = \Delta p / Q$ is

$$Z_{\text{paral}} = \frac{2Wh^3}{3\mu L} \ . \tag{53}$$

The shear stress distribution is

$$\tau_{\text{paral}} = \frac{\tau_w}{h} y , \tag{54}$$

where $\tau_w = \Delta p h / L$ is the wall shear stress at both plates.

4.1.2. Micro/nanofluids

Solution (50) of the same equation (49) at the velocity slip BC (13) with different slip coefficients at the upper and lower plates at the walls gives the parabolic velocity profile in the form

$$v_{\text{paral}}^{\text{slip}}(y) = \frac{\Delta p}{\mu L}\left(\frac{h^2}{2} + \frac{\beta_1\alpha_2 + \beta_2\alpha_1 + h(\beta_1 + \beta_2 + 2\alpha_1\alpha_2) - h^2(\alpha_1 - \alpha_2)}{2h + (\alpha_1 + \alpha_2)} + \right.$$
$$\left. + \frac{\beta_1 - \beta_2 + h(\alpha_1 - \alpha_2)}{2h + (\alpha_1 + \alpha_2)} y - \frac{y^2}{2} \right), \tag{55}$$

$$Q_{paral}^{slip} = \frac{2}{3}\frac{\Delta p h W}{\mu L}\left(\frac{2h^2(h-\alpha_1+\alpha_2)}{2h+(\alpha_1+\alpha_2)} + \right.$$
$$\left. + \frac{3h(\beta_1+\beta_2+2\alpha_1\alpha_2)+3(\beta_1\alpha_2+\beta_2\alpha_1)}{2h+(\alpha_1+\alpha_2)} \right), \quad (56)$$

$$Z_{paral}^{slip} = \frac{3\mu L}{2hW}\frac{2h+(\alpha_1+\alpha_2)}{2h^2(h-\alpha_1+\alpha_2)+3h(\beta_1+\beta_2+2\alpha_1\alpha_2)+3(\beta_1\alpha_2+\beta_2\alpha_1)}, \quad (57)$$

$$\tau_{paral}^{slip} = \frac{\tau_w}{h}\left(\frac{\beta_1-\beta_2+h(\alpha_1-\alpha_2)}{2h+(\alpha_1+\alpha_2)} - y \right). \quad (58)$$

The relationships (55), (56) for the simplified case $\alpha_1 = \alpha_2$, $\beta_1 = \beta_2$ of two plates with the same roughness have been presented in [5]. The general case has been studied in [4].

Comparative study of (55) and (51), (56) and (52), (58) and (54) revealed the following differences in the velocity profiles

$$v_{paral}^{slip}(y) - v_{paral}(y) = \frac{\Delta p}{\mu L(2h+(\alpha_1+\alpha_2))}\left(\beta_1\alpha_2+\beta_2\alpha_1 + \right.$$
$$\left. + h(\beta_1+\beta_2+2\alpha_1\alpha_2) - h^2(\alpha_1-\alpha_2) + (\beta_1-\beta_2+h(\alpha_1-\alpha_2))y \right), \quad (59)$$

volumetric flow rates

$$Q_{paral}^{slip} - Q_{paral} = \frac{2}{3}\frac{\Delta p h W}{\mu L}\left(\frac{h^2(\alpha_2-3\alpha_1)}{2h+(\alpha_1+\alpha_2)} \right.$$
$$\left. + \frac{3h(\beta_1+\beta_2+2\alpha_1\alpha_2)+3(\beta_1\alpha_2+\beta_2\alpha_1)}{2h+(\alpha_1+\alpha_2)} \right), \quad (60)$$

and shear stress

$$\tau_{paral}^{slip} - \tau_{paral} = \frac{\tau_w(\beta_1-\beta_2+h(\alpha_1-\alpha_2))}{h(2h+(\alpha_1+\alpha_2))}. \quad (61)$$

Individual task: Analyze the expressions (59)-(61) and determine the conditions on the coefficients α_1, α_2, β_1, β_2 which provide higher flow rate and lower shear stress due to the velocity slip at the walls. Build the plots for (51)–(54) similar to the ones presented in Fig. 5a–c, and the plots (59)–(61) (Fig. 6a–c) and compare them. Derive conclusions on physical behavior of the flows with no-slip, first order slip (microfluids) and second order slip (nanofluids) BC.

4.2. Laminar flow through a circular tube

4.2.1. Classical fluids

The pressure-driven ($\Delta p = p^+ - p^-$) axisymmetric ($\partial/\partial\theta = 0$) laminar flow $\vec{v} = (v_r, v_\theta, v_x) = (0, 0, v)$ through the tube of radius R and length L along its axis 0x (Fig. 9a) is considered. Cylindrical system of coordinates is associated with the tube.

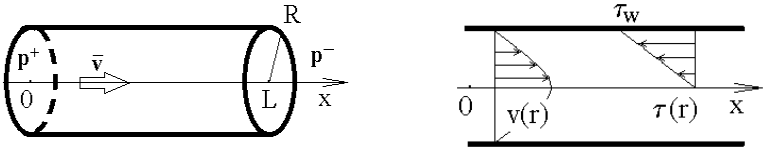

a *b*

Fig. 9. Pressure-driven laminar flow through a circular tube (a) with parabolic velocity and linear shear stress profiles (b)

The incompressibility condition gives again $v_x = v(r)$. Check that $(\vec{v}\cdot\nabla)\vec{v} = 0$ in this case. Projection of the steady flow momentum equations (3) in the cylindrical coordinates on the axis 0r gives $\partial p/\partial r = 0$, i. e. $p = p(x)$. From the inlet and outlet pressure values one can obtain the same dependence (51) with linear pressure distribution.

Projection of the momentum equation onto the axis 0x gives

$$\mu \frac{1}{r}\frac{d}{dr}\left(r\frac{dv(r)}{dr}\right) = \frac{\Delta p}{L}. \tag{62}$$

Integration of (62) with no-slip BC at the wall and symmetry of the velocity profile at the axis

$$v\big|_{r=R} = 0, \quad \left.\frac{dv}{dr}\right|_{r=0} = 0, \tag{63}$$

gives the following solution on the parabolic velocity profile, volumetric flow rate, hydraulic resistivity of the tube and shear stress (Fig. 9b):

$$v_{circ} = v_{max}\left(1 - \frac{r^2}{R^2}\right), \tag{64}$$

$$Q_{circ} = \frac{\Delta p}{8\mu_{eff} L}\pi R^4, \tag{65}$$

$$Z_{circ} = \frac{8\mu_{eff} L}{\pi R^4}, \tag{66}$$

$$\tau_{circ} = \tau_{wall}\frac{r}{R}, \tag{67}$$

where $v_{max} = \Delta p R^2/(4\mu_{eff} L)$, $\tau_{wall} = -\Delta p R/2L$.

4.2.2. Micro/nanofluids

Integration of (62) with BC (13) gives the following repressions for the velocity, flow rate, hydraulic resistivity and shear stress

$$v_{circ}^{slip}(r) = \frac{\Delta p R^2}{4\mu L}\left(1-\left(\frac{r}{R}\right)^2 + 2\frac{\beta+\alpha R}{R^2}\right), \tag{68}$$

$$Q_{circ}^{slip} = \frac{\Delta p}{8\mu L}\pi R^2\left(R^2 + 4(\beta+\alpha R)\right), \tag{69}$$

$$Z_{circ}^{slip} = \frac{\Delta 8\mu L}{\pi R^2\left(R^2 + 4(\beta+\alpha R)\right)}, \tag{70}$$

$$\tau_{circ}^{slip} = \tau_{circ}. \tag{71}$$

where α, β are the slip coefficients for the circular wall.

The relationships (68), (69), (71) are derived and analyzed in [5]. The corresponding differences in the flow parameters are:

$$v_{circ}^{slip}(r) - v_{circ}(r) = \frac{\Delta p(\beta+\alpha R)}{2\mu L}, \tag{72}$$

$$Q_{circ}^{slip} - Q_{circ} = \frac{\Delta p \pi R^2(\beta+\alpha R)}{2\mu L}, \tag{73}$$

$$Z_{circ} - Z_{circ}^{slip} = \frac{\Delta 8\mu L}{\pi R^2}\frac{4(\beta+\alpha R)}{(R^2 + 4(\beta+\alpha R))}. \tag{74}$$

Therefore, the slip flows through the circular tubes always have higher volumetric flow rates at the same pressure drop, i.e. lower hydraulic resistivity that in the no-slip flows.

4.3. Laminar flow in the annulus between two coaxial tubes

4.3.1. Classical fluids

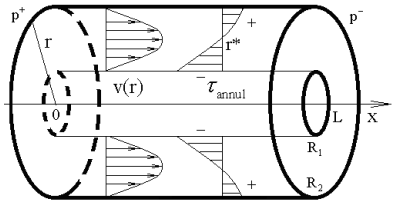

Fig. 10. Schema of the Poiseuille flow between coaxial cylinders with velocity and shear stress profiles

The same laminar $\vec{v} = (v_r, v_\theta, v_x) = (0, 0, v)$ pressure-driven steady ($\partial/\partial t = 0$) axisymmetric ($\partial/\partial\theta = 0$) flow through the annulus between the concentric tubes with long axis 0x and radiuses R_1 and R_2 is considered (Fig. 10).

The incompressibility condition gives $v = v(r)$; the non-linear term in (3) is absent ($(\vec{v}\cdot\nabla)\vec{v} = 0$). The pressure has the same linear distribution (51). Solution of (62) with no-slip BC at both walls

$$v\big|_{r=R1} = 0,\ v\big|_{r=R2} = 0 \tag{75}$$

is

$$v_{annul}(r) = \frac{\Delta P R_1^2}{4\mu_{eff} L}\left(1 - r^2 + \frac{\wp^2 - 1}{\ln(\wp)}\ln\left(\frac{r}{R_1}\right)\right), \tag{76}$$

$$Q_{annul} = \frac{\pi\Delta p R_1^4}{8\mu_{eff} L}\left(\wp^4 - 1 - \frac{(\wp^2 - 1)^2}{\ln(\wp)}\right), \tag{77}$$

$$Z_{annul} = \frac{8\mu_{eff} L \ln(\wp)}{\pi R_1^4\left(\ln(\wp)(\wp^2 + 1) - (\wp^2 - 1)\right)(\wp^2 - 1)}, \tag{78}$$

$$\tau_{annul} = \frac{\Delta P R_1^2}{4L}\left(\frac{\wp^2 - 1}{\ln(\wp)}\frac{1}{r} - 2r\right), \tag{79}$$

where $\wp = R_2 / R_1 > 1$.

The velocity (76) is maximal and the shear stress (79) is zero

$$v_{annul} = v_{max} \equiv \frac{\Delta P R_1^2}{4\mu L}\left(\wp^2 - \frac{\wp^2 - 1}{2\ln\wp}\left(1 - \ln\frac{\wp^2 - 1}{\ln\wp}\right)\right), \qquad \tau_{annul} = 0,$$

when $r = r^* = R_1\sqrt{\dfrac{\wp^2 - 1}{2\ln\wp}}$ (Fig.10).

4.3.2. Micro/nanofluids

When the flow is subjected to the slip BC (13) with different slip coefficients at the inner and outer walls, the integration of (62) with BC (13) at both walls with different slip coefficients will be:

$$\begin{aligned} v_{annul}^{slip}(\bar{r}) = \frac{\Delta P R_1^2}{4\mu LA}\Big((1 - 2\tilde{\alpha}_1 + 2\tilde{\beta}_1)(\wp\ln\wp - \alpha_2) - \wp(\wp^2 - 2\tilde{\alpha}_2\wp + 2\tilde{\beta}_2)\times \\ \times(\ln\wp - \tilde{\alpha}_1)(\wp^2 - 1 + 2(\tilde{\alpha}_1 - \tilde{\alpha}_2\wp + \tilde{\beta}_2 - \tilde{\beta}_1))\wp\ln(\bar{r}) - \bar{r}^2\Big), \end{aligned} \tag{80}$$

$$\begin{aligned} Q_{annul}^{slip} = \frac{\pi\Delta p R_1^4}{8\mu LA}\Big(2((1 - 2\tilde{\alpha}_1 + 2\tilde{\beta}_1)(\wp\ln\wp - \tilde{\alpha}_2) - \wp(\wp^2 - 2\tilde{\alpha}_2\wp + 2\tilde{\beta}_2)\times \\ \times(1 - \tilde{\alpha}_1))(\wp^2 - 1) + \frac{\wp}{2}(\wp^2 - 1 + 2(\tilde{\alpha}_1 - \tilde{\alpha}_2\wp + \tilde{\beta}_2 - \tilde{\beta}_1))\times \\ \times\left(2\wp^2\ln\wp - \wp^2 - 1\right) - (\wp^4 - 1)\Big), \end{aligned} \tag{81}$$

$$\tau_{annul}^{slip} = \frac{\Delta P}{4LA}\left(\frac{\wp}{\bar{r}}(\wp^2 - 1 + 2(\tilde{\alpha}_1 - \tilde{\alpha}_2\wp + \tilde{\beta}_2 - \tilde{\beta}_1)) - 2\bar{r}\right), \quad (82)$$

where $A = \wp\ln(\wp) + \tilde{\alpha}_1\wp - \tilde{\alpha}_2$, $\bar{r} = r / R_1$.

In this case, v_{annul}^{slip} reaches its maximum at

$r = r^{**} = R_1\sqrt{\frac{\wp^2 - 1 + 2(\tilde{\alpha}_1 - \tilde{\alpha}_2\wp + \tilde{\beta}_2 - \tilde{\beta}_1)}{2(\ln(\wp) + \tilde{\alpha}_1 - \tilde{\alpha}_2 / \wp)}}$, and $r^{**} > r^*$ or $r^{**} < r^*$ depending on the slip coefficients $\alpha_{1,2}$, $\beta_{1,2}$ and radii $R_{1,2}$. Like in the circular tubes, one can obtain $Q_{annul}^{slip} > Q_{annul}$ by a proper choice of the walls' parameters $\alpha_1, \alpha_2, \beta_1, \beta_2$ depending on the radii R_1, R_2. In [5] the solution (80)–(82) is presented in the simplified form at $\alpha_1 = \alpha_2$ and $\beta_1 = \beta_2$.

Individual task: Analyze the expressions (80)–(82) and determine the conditions on the coefficients $\tilde{\alpha}_{1,2}$, $\tilde{\beta}_{1,2}$ which provide higher flow rate and lower shear stress due to the velocity slip at the walls. Build the plots for (80)–(82) in comparison to the plots for (76)–(79) and analyze them. Derive conclusions on physical behavior of the flows with no-slip, first order slip ($\alpha_1 \neq 0, \beta_1 = 0$, microfluids) and second order slip ($\alpha_1 \neq 0, \beta_1 \neq 0$, nanofluids) BC.

4.4. Laminar flow through a tube with elliptic cross-section

4.4.1. Classical fluids

Let us consider similar pressure-driven laminar flow through the tube with axis 0z and elliptic cross-section

$$\frac{x^2}{a^2} + \frac{y^2}{b^2} = 1 \quad (83)$$

with semi-major axis a and b. The velocity no-slip BC will be satisfied if one will search for the solution of (2), (3) in the form

$$v_{elliptic}(x, y) = A\left(1 - \frac{x^2}{a^2} - \frac{y^2}{b^2}\right), \quad A = \text{const.} \quad (84)$$

Substitution of (84) into (62) gives for the constant A the following expression

$$A = \frac{\Delta p}{2\mu_{eff} L}\frac{a^2 b^2}{a^2 + b^2}. \quad (85)$$

As it is clear from (84), $A = v_{elliptic}\big|_{x,y=0} = V_{max}$.

Integration of (84), (85) over the elliptic cross-section give the volumetric flow rate in the form

$$Q_{elliptic} = \frac{\pi a^3 b^3 \Delta p}{4\mu_{eff} L(a^2 + b^2)}. \quad (86)$$

As one can see from comparison of (64) and (84), when $a = b = R$, the formulae (64) and (84) coincide. The same is valid for the formulae (65) and (86).

The viscous (shear) stress tensor

$$\tau_{ik} = \frac{1}{2}\left(\frac{\partial v_i}{\partial x_k} + \frac{\partial v_k}{\partial x_i}\right) \quad (87)$$

has 4 non-zero components

$$\tau_{xz} = \tau_{zx} = \frac{\Delta p}{L}\frac{b^2 x}{a^2 + b^2} \text{ and } \tau_{yz} = \tau_{zy} = \frac{\Delta p}{L}\frac{a^2 y}{a^2 + b^2} \quad (88)$$

with maximal shear stress values at the walls

$$\max\{\tau_{xz}, \tau_{zx}\} = \frac{\Delta p}{L}\frac{ab^2}{a^2 + b^2}, \ \max\{\tau_{yz}, \tau_{zy}\} = \frac{\Delta p}{L}\frac{a^2 b}{a^2 + b^2} \quad (89)$$

and

$$\max|\tau_z| = \frac{\Delta p}{L}\frac{a^2 b^2}{a^2 + b^2}. \quad (90)$$

When $a = b = R$, (88)-(90) coincide with (67).

4.4.2. Micro/nanofluids

Since in the case of the conventional and micro/nanofluids the solutions (64) and (68) differ by a constant, the velocity slip solutions of (2)–(3) for the elliptic tubes can also be found in the form (84) with the differences by constants in the form

$$v^{slip}_{elliptic}(x, y) = A_1\left(1 - \frac{x^2 + A_2}{a^2} - \frac{y^2 + A_3}{b^2}\right), \quad A_{1,2,3} = \text{const}. \quad (91)$$

Then substitution of (91) into (62) gives the velocity field

$$v^{slip}_{elliptic}(x, y) = V_{max}\left(1 - \frac{x^2 + 2(\alpha a - \beta)}{a^2} - \frac{y^2 + 2(\alpha b - \beta)}{b^2}\right). \quad (92)$$

When $a = b = R$, (92) coincides with (68). Integration of (92) over the elliptic cross-section gives the volumetric flow rate

$$Q^{slip}_{elliptic} = Q_{elliptic}\left(1 + \frac{\beta - \alpha a}{a^2} + \frac{\beta - \alpha b}{b^2}\right). \quad (93)$$

When $a = b = R$, (93) coincides with the expression (69) for the circular flow with velocity slip.

In this case the shear stress field keeps the same non-zero coefficients (89)–(90) because the corresponding differences in the velocities are constants that disappear in the differentials (87).

Individual task: Analyze the expressions (92)–(93) in comparison to (84), (86) and determine the conditions on the coefficients α_1, β_1 which provide higher flow rate and lower shear stress due to the velocity slip at the walls, i.e. the lower hydraulic ressitivities of the elliptic channels with the velocisy slip BC in comparison to the velocity no-slop BC. Build the plots for (92)–(93) in comparison to the plots for (84)–(86) and analyze them. Derive your conclusions on physical behavior of the flows with no-slip, first order slip (microfluids, $\alpha_1 \neq 0, \beta_1 = 0$) and second order slip (nanofluids, $\alpha_1 \neq 0, \beta_1 \neq 0$) BC.

4.5. Laminar flow through a tube with equilateral triangle cross-section

4.5.1. Classical fluids

Let us consider the case when the prismatic channel has the cross-section as an equilateral triangle with the axis 0x and the sides $y = 0$ (base of the channel), $y = a\sqrt{3}/2 \pm \sqrt{3}z$ (left and right sides), and with the longitudinal axis 0z. The same trick as one used in the solution (84) in comparison to the solution (64) can be used here to obtain zero velocity at the three sides of the triangle, namely

$$v_{\Delta}(y,z) = Ay\left(y - \frac{a\sqrt{3}}{2} - \sqrt{3}z\right)\left(y - \frac{a\sqrt{3}}{2} + \sqrt{3}z\right), \; A = \text{const.} \qquad (94)$$

Substitution of (94) into (3) gives

$$A = \frac{\Delta p}{2\sqrt{3}\mu_{\text{eff}} La}, \quad v(y,z) = \frac{\Delta p \cdot y}{2\sqrt{3}\mu_{\text{eff}} La}\left(\left(y - \frac{a\sqrt{3}}{2}\right)^2 - 3z^2\right), \qquad (95)$$

while the pressure distribution still corresponds to (51).

An example of the velocity distribution (95) is given in Fig. 11.

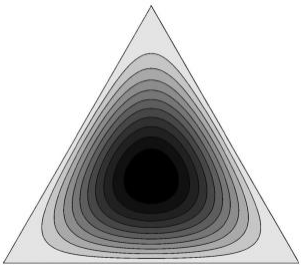

Fig. 11. Contours of the fluid velocity profile across the triangle cross section of the channel. The darker regions correspond to higher velocities

Integration of (94) over the triangle cross-section gives the volumetric flow rate

$$Q = \frac{a^4\sqrt{3}\Delta p}{320\mu_{\text{eff}} L}. \qquad (96)$$

Individual task: Using (87) and (94), compute the shear stress

$$\tau_{\Delta} = \sqrt{\tau_{xz}^2 + \tau_{xy}^2} \qquad (97)$$

distribution in the flow and at the three walls.

4.5.2. Micro/nanofluids

Individual task: Find out the solution $v_{\Delta}^{slip}(y,z)$ for the flow velocity in the triangle channel with slip BC. In the most general case the three walls of the channel have different sets of the roughness parameters α_1,β_1, α_2,β_2, α_3,β_3. Try the same approach that had been used for the elliptic tubes, i. e. substitute the expression

$$v_{\Delta}^{slip}(y,z) = A(y + A_1)\left(y - \frac{a\sqrt{3}}{2} - \sqrt{3}z + A_2\right)\left(y - \frac{a\sqrt{3}}{2} + \sqrt{3}z + A_3\right) \qquad (98)$$

into the Navier-Stokes equations (3) and find out the expressions for A_{1-3}.

Compute the volumetric flow rate

$$Q_{\Delta}^{slip} = 2\int_0^{\frac{a\sqrt{3}}{2}} dy \int_0^{\frac{y}{\sqrt{3}}-\frac{a\sqrt{3}}{2}} v_{\Delta}^{slip} dz\,. \qquad (99)$$

Compute the values of the shear stress vectors

$$\tau_{\Delta}^{slip} = \sqrt{\tau_{xz}^2 + \tau_{xy}^2} \qquad (100)$$

in the flow and at the walls.

Determine the conditions on the coefficients $\alpha_1,\alpha_2,\alpha_3,\beta_1,\beta_2,\beta_3$ which provide higher flow rate and lower shear stress due to the velocity slip at the walls, i.e. the lower hydraulic resistivity of the triangle channel with the velocisy slip BC in comparison to the velocity no-slip BC. Build the plots for (98) – (100) in comparison to the plots for (95) – (97) and analyze them. Derive your conclusions on physical behavior of the flows with no-slip, first order slip (microfluids, $\alpha_{1-3} \neq 0,\ \beta_{1-3} = 0$) and second order slip (nanofluids, $\alpha_{1-3} \neq 0,\ \beta_{1-3} \neq 0$) BC.

4.6. Laminar flow through a tube with rectangle cross-section

4.6.1. Classical fluids

Let us consider the laminar flow through a channel with the axis 0x and rectangle cross section $z \in [-h,h]$, $y \in [-\chi h, \chi h]$ where χ is the aspect ratio (width to height ratio) of the channel. Then the solution of (3) can be found as Fourier expansions in $\cos\left(\frac{2n+1}{h}\pi z\right)$ that satisfies the no-slip BC. Substitution in (2),(3) gives the flow distribution

$$v_{\square}(y,z) = \frac{4\Delta p h^2}{\pi^3 \mu_{eff} L}\sum_{n=0}^{\infty}\frac{(-1)^n}{(2n+1)^3}\left[1 - \frac{\mathrm{ch}\left(\frac{2n+1}{2}\frac{\pi y}{h}\right)}{\mathrm{ch}\left(\frac{2n+1}{2}\pi\chi\right)}\right]\cos\left(\frac{2n+1}{h}\pi z\right). \qquad (101)$$

An example of the velocity distribution (101) across a rectangle cross section is given in Fig. 12a. Integration of (101) over the rectangle cross section gives the flow rate

$$Q_{\square} = \frac{\Delta p h^4}{4\mu_{eff} L}\left(\frac{16}{3}\chi - \frac{1024}{\pi^5}\sum_{n=0}^{\infty}\frac{1}{(2n+1)^5}\,\mathrm{th}\left(\frac{2n+1}{2}\pi\chi\right)\right). \qquad (102)$$

The non-zero components of the shear stress tensor (87) are

$$\tau_{xz} = \tau_{zx} = \frac{\mu_{\text{eff}}}{2}\frac{\partial \mathrm{v}_{\square}}{\partial \mathrm{z}} =$$

$$= -\frac{4\Delta \mathrm{ph}}{\pi^2 \mathrm{L}}\sum_{\mathrm{n}=0}^{\infty}\frac{(-1)^{\mathrm{n}}}{(2\mathrm{n}+1)^2}\left[1 - \frac{\mathrm{ch}\left(\frac{2\mathrm{n}+1}{2}\frac{\pi \mathrm{y}}{\mathrm{h}}\right)}{\mathrm{ch}\left(\frac{2\mathrm{n}+1}{2}\pi\chi\right)}\right]\sin\left(\frac{2\mathrm{n}+1}{\mathrm{h}}\pi \mathrm{z}\right), \qquad (103)$$

$$\tau_{xy} = \tau_{yx} = \frac{\mu_{\text{eff}}}{2}\frac{\partial \mathrm{v}_{\square}}{\partial \mathrm{y}} =$$

$$= \frac{2\Delta \mathrm{ph}}{\pi^2 \mathrm{L}}\sum_{\mathrm{n}=0}^{\infty}\frac{(-1)^{\mathrm{n}}}{(2\mathrm{n}+1)^2}\frac{\mathrm{sh}\left(\frac{2\mathrm{n}+1}{2}\frac{\pi \mathrm{y}}{\mathrm{h}}\right)}{\mathrm{ch}\left(\frac{2\mathrm{n}+1}{2}\pi\chi\right)}\cos\left(\frac{2\mathrm{n}+1}{\mathrm{h}}\pi \mathrm{z}\right). \qquad (104)$$

The values of the shear stress vectors

$$\tau_{\square} = (\tau_{xy}^2 + \tau_{xz}^2)^{1/2} \qquad (105)$$

computed on (101), (105) are presented in Fig. 12a,b.

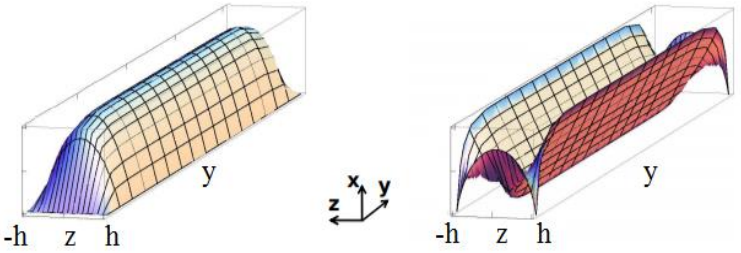

a *b*

Fig. 12. Velocity (a) and shear stress (b) distributions across the channel with rectangular cross section

4.6.2. Micro/nanofluids

Individual task: Find out the solution $\mathrm{v}_{\square}^{\mathrm{slip}}(\mathrm{y},\mathrm{z})$ for the flow velocity in the rectangle channel with slip BC. In the most general case the four walls of the channel have different sets of the roughness parameters α_1, β_1, α_2, β_2, α_3, β_3,

α_4, β_4 .Try the same approach that had been used for the elliptic and triangle tubes, i. e. substitute the expression

$$v_{\square}^{slip}(y,z) = \frac{4\Delta p h^2}{\pi^3 \mu_{eff} L} \sum_{n=0}^{\infty} \frac{(-1)^n}{(2n+1)^3} \left[1 - \frac{\mathrm{ch}\left(\frac{2n+1}{2} \frac{\pi y}{h} \right)}{\mathrm{ch}\left(\frac{2n+1}{2} \pi \chi \right)} + A_1 \right] \left[\cos\left(\frac{2n+1}{h} \pi z \right) + A_2 \right] \qquad (106)$$

into the Navier-Stokes equations (3) and find out the expressions for $A_{1,2}$.

Compute the volumetric flow rate by integration of (106) over the rectangle cross section of the channel. Compute the shear stress distribution n the channel and over its walls.

Determine the conditions on the coefficients $\alpha_1, \alpha_2, \alpha_3, \alpha_4, \beta_1, \beta_2, \beta_3, \beta_4$ which provide higher flow rate and lower shear stress due to the velocity slip at the walls, i. e. the lower hydraulic resistivity of the rectangle channels with the velocity slip BC in comparison to the velocity no-slop BC. Build the plots based on (106) in comparison to the plots for (101), (102), (105) and analyze them. Derive your conclusions on physical behavior of the flows with no-slip, first order slip (microfluids $\alpha_{1-4} \neq 0,\ \beta_{1-4} = 0$) and second order slip (nanofluids, $\alpha_{1-4} \neq 0,\ \beta_{1-4} \neq 0$) BC.

REFERENCES

1. MEMS Microfluidics for Lab-on-a-Chip. Applications, Microelectromechanical Systems and Devices. N. Islam (ed.). – InTech, 2012.
2. MEMS Materials and Processes Handbook. R. Ghodssi and P. Lin (eds.). Springer, 2011.
3. Liou W., Fang Y. Microfluid Mechanics: Principles and Modeling (Nanoscience and Technology). McGraw-Hill Education Publ., 2005.
4. Cherevko V. Complex flows of immiscible microfluids and nanofluids with velocity slip bounary conditions / V. Cherevko, N. Kizilova // Nanophysics, Nanomaterials, Interface Studies, and Applications, Springer Proceedings in Physics. 2017. Vol. 183 / eds. O. Fesenko, L. Yatsenko. P. 207–230.
5. Karniadakis G. E. Microflows and nanoflows: Fundamentals and simulation / G. E. Karniadakis, A. Beskok, N. Aluru // Interdisc. Appl. Math. Series. 2005. Vol. 29. Springer-Science.
6. Neto C. Boundary slip in Newtonian liquids: a review of experimental studies / C. Neto, D. R. Evans, E. Bonaccurso et al. // Rep. Prog. Phys. 2005. Vol. 68. P. 2859–2897.
7. Bechert D. W. Fluid mechanics of biological surfaces and their technological application / D. W. Bechert, M. Bruse, W. Hage, R. Meyer // Naturwissenschaften. 2004. Vol. 87. P. 157–171.
8. Christodoulou K. N., Scriven L. E. The fluid mechanics of slide coating / K. N. Christodoulou, L. E. Scriven // J. Fluid Mech. 1992. Vol. 99. P. 39–55.
9. Beavers G. S. Boundary conditions at a naturally permeable wall // J. Fluid Mech. 1967. Vol. 30. P. 197–207.
10. Denn M. M. Issues in viscoelastic fluid mechanics // Annu. Rev. Fluid Mech. 1990. Vol. 22. P. 13–34.
11. Mohammadi B., Pironneau O. Analysis of the k–ε turbulence model. Wiley, 1974.
12. Sbragaglia M., Prosperetti A. Effective velocity boundary condition at a mixed slip surface // J. Fluid Mech. 2007. Vol. 578. P. 435–451.
13. Sidik N. A. C. A review on preparation methods and challenges of nanofluids, Intern. Communic / N. A. C. Sidik, H. A. Mohammed, O. A. Alawi, S. Samion // Heat Mass Transfer. 2014. Vol. 54. P. 115–125.
14. Lim C. Y. Application of lattice Boltzmann method to simulate microchannel flows / C. Y. Lim, C. Shu, X. D. Niu, Y. T. Chew // Phys. Fluids. 2002. Vol. 14. P. 2299–2308.
15. Mala G. M., Li D. Q. Flow characteristics of water in microchannels / Int. J. Heat Fluid Flow. 1999. Vol. 20. P. 142–148.
16. Tang G. H. Experimental study of compressibility, roughness and rarefaction influences on microchannel flow /G. H. Tang, Z. Li, Y. L. He, W. Q. Tao // Intern. J. Heat Mass Transfer. 2007. Vol. 50. P. 2282–2295.
17. Rice C. L. Electrokinetic flow in a narrow cylindrical capillary / C. L. Rice, R. Whitehead // J. Phys. Chem. 1965. Vol. 69. P. 4017–4021.

18. Kizilova N. Space-filling trees for microfluidic applications. A review / N. Kizilova // Nanoplasmonics, Nano-Optics, Nanocomposites, and Surface Studies. Springer Proceedings in Physics / O. Fesenko, L. Yatsenko (eds.). 2015. P. 7–23
19. Gad-el-Hak M. MEMS Introduction and fundamentals / M. Gad-el-Hak. The MEMS Handbook. Second ed. Taylor & Francis Group, LLC, 2006.
20. Zhang W.-M., Meng G., Wei X., A review on slip models for gas microflows // Microfluid. Nanofluid. 2012. Vol. 13. P. 845–882.
21. Wu P.Y. Measurement of the friction factors for the flow of gases in very fine channels used for microminiature Joule–Thomson refrigerators / P. Y. Wu, W. A. Little // Cryogenics. 1983. Vol. 23. P. 273–277.
22. Urbanek W. An investigation of the temperature dependence of Poiseuille numbers in microchannel flow / W. Urbanek, J. N. Zemel, H. Bau // J. Micromech. Microeng. 1993. Vol. 3. P. 206–208.
23. Peng X. F. Frictional flow characteristics of water flowing through rectangular channels / X. F. Peng, G. P. Peterson, B. X. Wang // Exp. Heat Transfer. 1994. Vol. 7. P. 249–264.
24. Papautsky I. Effects of rectangular microchannel aspect ratio on laminar friction constant / I. Papautsky, B. K. Gale, S. Mohanty et al. // Proc. of the Society of Photo-optical Instrumentation Engineers (SPIE). 1999. Vol. 3877. P. 147–158.
25. Qu W. L. Pressure-driven water flows in trapezoidal silicon microchannels / W. L. Qu, G. M. Mala, D. Q. Li // Int. J. Heat Mass Transfer. 2000. Vol. 43 P. 353–364.
26. Wang H. Influence of three-dimensional wall roughness on the laminar flow in microtube / H. Wang, Y. Wang // Intern. J. Heat Fluid Flow. 2007. Vol. 28. P. 220–228.
27. Maninen M. On the mixture model for multiphase flow / M. Maninen, V. Taivassalo. VTT Publ., Espo. 1996.
28. Ghasemi B. Brownian motion of nanoparticles in a triangular enclosure with natural convection /B. Ghasemi, S. Aminossadati // Intern. J. Thermal Sci. 2010. Vol. 49. P. 931–940.
29. Merkle C. L. An analytical study of the effects of surface roughness on boundary-layer transition / C. L. Merkle, T. Kubota, D.R.S. Ko – Air Force Office of Scientific Research Space and Missile System Organization, AD/A004786, 1974.
30. Corcione M. Heat transfer features of buoyancy-driven nanofluids inside rectangular enclosures differentially heated at the sidewalls // Intern. J. Thermal Sci. 2010. Vol. 49. P. 1536–1546.
31. Malvandi A., Ganji D. D. Effects of nanoparticle migration and asymmetric heating on magnetohydrodynamic forced convection of alumina/water nanofluid in microchannels // European J. Mech. Ser. B. Fluids. 2015. Vol. 52. P. 169–184.

32. Mo G., Rosenberger F. Molecular-dynamics simulation of flow in a two-dimensional channel with atomically rough walls // Phys. Rev. Ser. A. 1990. Vol. 42. P. 4688–4892.
33. Chapman S., Cowling T. G. The Mathematical Theory of Non-uniform Gases. An Account of the Kinetic Theory of Viscosity, Thermal Conduction and Diffusion in Gases. Cambridge Math. Library, 1991.
34. Roohi E., Darbandi M. Extending the Navier–Stokes solutions to transition regime in two-dimensional micro- and nanochannel flows using information preservation scheme // Phys. Fluids. 2009. Vol. 21. P.082001.
35. Dongari N. Pressure-driven diffusive gas flows in micro-channels: from the Knudsen to the continuum regimes / N. Dongari, A. Sharma, F. Durst // Microfluid. Nanofluid. 2009. Vol. 6. P. 679–692.
36. Dongari N. Predicting microscale gas flows and rarefaction effects through extended Navier–Stokes–Fourier equations from phoretic transport considerations / N. Dongari, F. Durst, S. Chakraborty // Microfluid. Nanofluid. 2010. Vol. 9. P. 831–846.
37. Aubert C., Colin S. High-order boundary conditions for gaseous flows in rectangular microducts // Microscale Thermophys. Engin. 2001. Vol. 5. P. 41–54.
38. Landau L. D. Theoretical Physics. Fluid Mechanics / L. D. Landau, Ye. M. Lifshitz, Pergamon Press. Vol. 6. 2-nd edition Oxford. 1987. 539 p.